ADVANCED FUNCTIONAL MATERIALS
www.afm-journal.de
www.MaterialsViews.com

High Color Rendering Index Hybrid III-Nitride/Nanocrystals White Light-Emitting Diodes

Zhe Zhuang, Xu Guo, Bin Liu, Fengrui Hu, Yi Li, Tao Tao, Jiangping Dai, Ting Zhi, Zili Xie, Peng Chen, Dunjun Chen, Haixiong Ge, Xiaoyong Wang, Min Xiao, Yi Shi, Youdou Zheng, and Rong Zhang**

An excellent hybrid III-nitride/nanocrystal nanohole light-emitting diode (h-LED) has been developed utilizing nonradiative resonant energy transfer (NRET) between violet/blue emitting InGaN/GaN multiple quantum wells (MQWs) and various wavelength emitting nanocrystals (NCs) as color-conversion mediums. InGaN/GaN MQWs are fabricated into nanoholes by soft nanoimprint lithography to minimize the separation between MQWs and NCs. A significant reduction in the decay lifetime of excitons in the MQWs of the hybrid structure has been observed as a result of the NRET from the nitride emitter to NCs. The NRET efficiency of the hybrid structures is obtained from the decay curves, as high as 80%. Moreover, a modified Förster formulation has exhibited that the exciton coupling distance in the hybrid structures is less than the Förster's radius, demonstrating a strong coupling between MQWs and NCs. Finally, based on a systemic optimization for white emission indexes, a series of hybrid ternary complementary color h-LEDs have been demonstrated with a high color rendering index, up to 82, covering the white light emission at different correlated color temperatures ranging from 2629 to 6636 K, corresponding to warm white, natural white, and cold white.

1. Introduction

The need has been emphasized for efficient solid-state emitters in applications ranging from displays to solid-state lighting because they potentially provide substantial energy savings to allow for efficient energy utilization of limited energy resources.[1] The last decades have seen unprecedented achievements in the development of solid-state lighting gradually and ultimately leading to lighting sources mainly based on III-nitride semiconductors.[2] With regard to white light-emitting diodes (LEDs), the conventional approach is to mainly use blue emission from InGaN/GaN-based LEDs radiatively pumping down-conversion phosphor materials, such as $Y_3Al_5O_{12}:Ce^{3+}$ (YAG), to provide longer wavelength emission components. However, these white LEDs have a low color rendering index (CRI) and high correlated color temperature (CCT) owing to red emission deficiency in the visible spectrum.[3] In addition, other issues still require consideration such as the self-absorption of the phosphor, the low efficiency of the energy transfer from the blue LED to the down-conversion phosphor and the degradation of phosphors.[2,4,5]

To avoid these drawbacks by using abovementioned phosphors, scientists started to devote their efforts to developing phosphor-free white LEDs.[4] A variety of approaches such as multichip white LEDs, monolithic white LEDs, and color-conversion white LEDs have been extensively exploited.[5–7] Among them, color conversion is regarded as the most popular method, and many different materials have been used for color conversion in white light generation instead of phosphors.[2,8–15] Very recently, a novel organic energy down-converting material, $[BODFluTh]_2FB$, has been synthesized as an effective color converter for application in hybrid inorganic/organic white LEDs, the chromaticity coordinates of which are very close to the center of the chromaticity diagram where white light is located.[16] However, the CCT of this hybrid inorganic/organic white LED is still that of

Dr. Z. Zhuang, Prof. B. Liu, Dr. Y. Li, Dr. T. Tao, Dr. J. Dai, Dr. T. Zhi, Prof. Z. Xie, Prof. P. Chen, Prof. D. Chen, Prof. Y. Shi, Prof. Y. Zheng, Prof. R. Zhang
Jiangsu Provincial Key Laboratory of Advanced Photonic and Electronic Materials
School of Electronic Science and Engineering
Nanjing National Laboratory of Microstructures
Nanjing University
Nanjing 210093, P. R. China
E-mail: bliu@nju.edu.cn; rzhang@nju.edu.cn

Dr. X. Guo, Prof. H. Ge
College of Engineering and Applied Sciences
Nanjing National Laboratory of Microstructures
Nanjing University
Nanjing 210093, P. R. China

Dr. F. Hu, Prof. X. Wang, Prof. M. Xiao
School of Physics
Nanjing National Laboratory of Microstructures
Nanjing University
Nanjing 210093, P. R. China

DOI: 10.1002/adfm.201502870

cold white light, which is similar to the conventional approach with YAG yellow phosphors. Meanwhile, semiconductor nanocrystals (NCs) are also considered to be promising nanoscale color-selectable emitters and combine high photoluminescence (PL) quantum yields (QYs) with chemical flexibility and processibility.[1,17–24] Through hybridization of different NC combinations, it is quite convenient to adjust white light parameters, including the chromaticity coordinates, CCT, and CRI.[25,26] A hybrid white LED using NCs as down-conversion materials was previously demonstrated byChen et al., exhibiting a high CRI of 91 and a CIE-1931 coordinate of (0.33, 0.33).[27] However, this device is also based on a blue chip radiatively pumping green- and red-emitting NCs with a low color-conversion efficiency (CCE) because of large separation between the active layer in the LEDs and NCs.

To overcome this drawback, nonradiative energy transfer (NRET) was proposed as another method for color conversion.[1,2,11,22,28–33] Compared with the absorption-based radiative energy transfer approach mentioned above, the utilization of NRET is able to suppress energy loss associated with the intermediate light emission steps and increases the CCE.[1,11,22,29,30] The NC-based LED employing NRET was first demonstrated by a single monolayer of CdSe NCs assembled on top of an InGaN/GaN quantum well with a thin capping layer of only 3 nm to reduce the separation between CdSe NCs and the InGaN active layer, obtaining a significantly higher CCE than the values based on absorption-re-emission mentioned above.[1,11] However, this structure is not as practical for a standard LED with a 200 nm thick p-type layer. As a result, top-down dry-etched nanopillar[2,29,31,33] or nanohole III-nitride structures[30] have been introduced to form hybrid structures utilizing the NRET process. Hybrid III-nitride/organic semiconductor nanostructures have been demonstrated with nearly zero separation between blue light-emitting InGaN/GaN multiple quantum wells (MQWs) and a yellow light-emitting polymer material named F8BT, obtaining a high NRET efficiency.[2] However, the yellow emitting polymer used in this hybrid structure is easy to be photo-oxidized, which is not sufficiently stable for fabricating devices.

In this paper, we have realized white emission through the hybridization of highly ordered violet/blue nanohole LEDs (h-LEDs) and CdSe/ZnS core/shell NCs. The ordered nanohole structures have advantages in the following aspects. In the physical mechanism, first, the quantum confined Stark effect, which is generated by strain-induced polarization fields, can be eliminated or partially reduced, leading to an increased internal quantum efficiency.[34,35] Second, owing to ordered nanohole arrays serving as photonic crystals (although filling NCs reduces the difference of the refractive index for GaN/air interface, it still can be regarded as comprising photonic crystals), light extraction can be significantly enhanced compared to the planar structures.[36,37] Both advantages are similar to those of nanorod-based LEDs. Uniquely, for nanohole arrays in our case, the emission area of InGaN/GaN MQW structure is reduced only a small percentage and is 3.5 times larger than that of its counterpart nanorod arrays with the same size and separation. As expected for the nanohole-based hybrid structure, efficient NRET, with an efficiency as high as 80%, has been realized, which is nearly the same as other similar hybrid structures previously reported.[2,28,30] More importantly, the LED device fabrication process can benefit from the nanohole structures. The hybrid h-LEDs are patterned by our developed 2-in wafer-level soft UV-curing nanoimprint lithography (NIL) with cost efficiency and great precision,[38,39] and fabricated compatibly with current LED processes with no need for insulating material to fill gaps in nanorod-based LEDs.[35,40] As a result, with regard to device characterization, the indices of the hybrid h-LEDs, such as chromaticity coordinates CCT and CRI, can be conveniently modified the same way as those standard plane devices, resulting in the potential for mass production in the future.[25] Moreover, CdSe/ZnS core/shell NCs have stable luminescence over a long period of time in the air, which is important for practical applications.[17]

2. Results and Discussion

Figure 1a presents a schematic of the designed hybrid h-LED, showing that the ordered arrays of nanoholes are fabricated from planar InGaN/GaN MQW structures and penetrate through the active layers. To achieve good current spreading, the indium tin oxide (ITO) layer is deposited on the surface of LEDs and patterned into nanoholes as well. CdSe/ZnS core/shell NCs are then filled in these nanoholes as a down-conversion medium. Unlike conventional color-conversion LEDs, this structure can bring CdSe/ZnS core/shell NCs within the vicinity of the active MQWs. Figure 1b shows the scanning electron microscope (SEM) image of the bare violet InGaN/GaN nanohole arrays at a 30° inclined view. It is observed that these nanohole arrays with a diameter of 300 nm are in a hexagonal lattice whose lattice constant is 600 nm as designed. Figure 1c exhibits the cross section of the hybrid device filled with NCs in the nanoholes, approximately 1.2 μm in depth. From this figure, we can clearly see that the sidewalls of InGaN/GaN MQWs are closely surrounded by NCs as expected, which is essential for the NRET process (also see similar transmission electron microscope (TEM) characterizations from Figure S1 in Supporting Information). It is worth mentioning that on the p-GaN, there is an ITO cladding layer to serve as a current spreading layer, which is also patterned and fabricated to nanoholes as shown in both Figure 1b,c. The morphology of the CdSe/ZnS core/shell NCs is shown in Figure 1d, and the diameter of these NCs is within 10 nm (see Table S1 in the Supporting Information).

Although these NCs are originally insulated, it still should be carefully determined whether the filling of NCs has any impact on the electrical performance of the hybrid LED devices. **Figure 2**a shows the *I–V* characteristics of the blue h-LED with and without NCs. The inset in Figure 2a presents the *I–V* curve at the reverse bias on a logarithmic scale. It can be demonstrated that the h-LED exhibits a typical *p–n* junction diode. With increasing voltage, the current is stably increased. The measured *I–V* characteristics at room temperature (RT) show a sharp onset voltage at 4.5 V in the forward bias with relatively negligible leakage current at the reverse bias, which benefits from a mostly compatible LED fabrication process. From this figure, it can be clearly seen that the *I–V* curve has no change at all after drop casting NCs to the h-LEDs, which

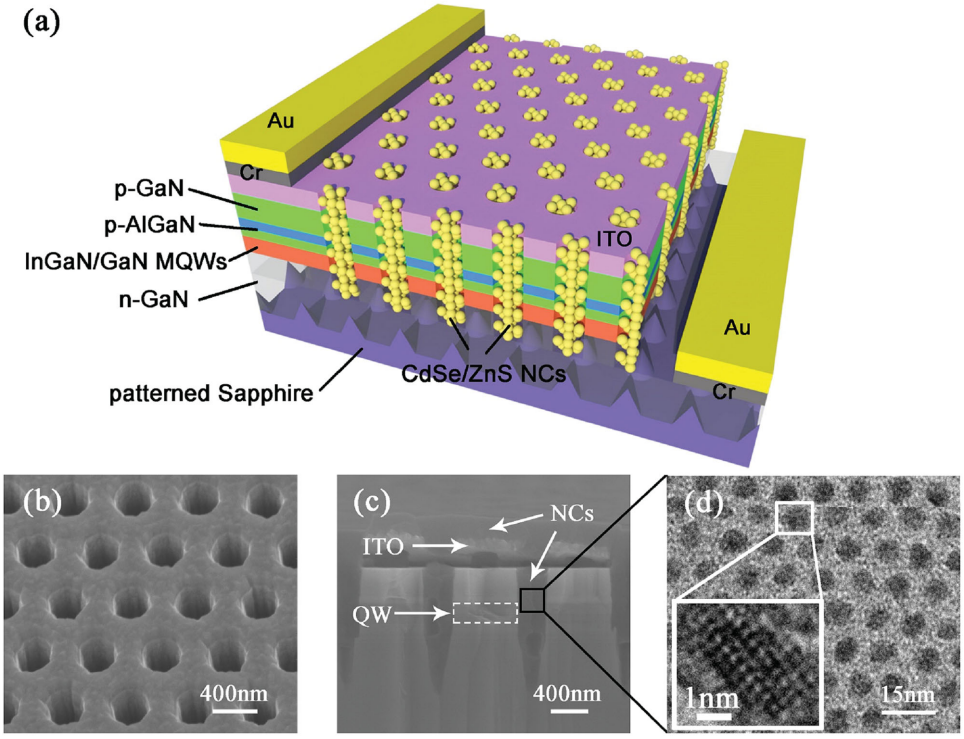

Figure 1. a) Schematic diagrams of hybrid h-LED. b) Bird's eye view SEM image of ordered nanohole arrays in the absence of NCs with ITO current spreading layer on the surface. c) Cross-sectional view SEM image of nanoholes filled with NCs and d) TEM image of CdSe/ZnS core/shell NCs and a high-resolution image in the inset.

definitely illustrates that NCs have no influence on the injection of electrons and holes. The inset image in Figure 2b is the appearance of the bare blue h-LEDs at the injection current of 1 mA, revealing excellent current spreading and luminescence uniformity due to the nanohole ITO layer, which is much better than previously reported nanorod-[29] or nanohole-based[30] LEDs used in hybrid structures. Moreover, the electroluminescence (EL) spectra of the bare h-LEDs at the injection current ranging from 1 to 80 mA are measured as well (not shown here), and no evidence of device degradation is observed. Based on these EL spectra, the EL integral intensity as a function of the increasing injection current is extracted, as shown in Figure 2b on a logarithmic scale. This clearly shows that the EL integral intensity scales linearly with injection current and slightly saturates over the injection current of 40 mA. This linear relationship between EL integral intensity and injection current implies that a high density of excitons are formed in nanohole MQWs (h-MQWs) when carriers are injected,[11,30] ensuring that excitons in h-MQWs and NCs can strongly couple via NRET.

To further explore the optical properties of the hybrid h-LED, the EL emission of violet/blue h-LEDs with three types of NCs are measured at the injection current of 20 mA, as shown in Figure 2c,d. Because the PL emission peaks of these NCs are 546, 586, and 621 nm (see Figure S2 in the Supporting Information), they are respectively named as 546-NCs, 586-NCs, and 621-NCs for simplicity. The violet square line in Figure 2c and the blue square line in Figure 2d show the EL spectra of the bare violet and blue h-LEDs, respectively. The other orange circle, green regular triangle, and red inverted triangle lines depict the EL spectra of hybrid violet or blue h-LEDs with 546-NCs, 586-NCs, and 621-NCs, respectively. It can be clearly seen that those NCs have been pumped by the electrically driven h-LEDs and emitted a longer-wavelength light. To evaluate the color-conversion ability of the hybrid h-LEDs, CCE (η_c) is defined as the ratio of the integral emission intensity of NCs in the hybrid h-LED (I_{NC}^{H}) to that of the bare h-LED without NCs (I_{MQW}), $\eta_c = I_{NC}^{H} / I_{MQW}$. As a result, the CCE of hybrid violet and blue h-LED filled with 546-NCs is as high as 69% and 37%, respectively. (for other data, see Table S2 in the Supporting Information.) In addition, another important parameter, the effective QY of NC emission, $\eta_{QY}^{*} = I_{NC}^{H} / \left(I_{MQW} - I_{MQW}^{H}\right)$, is also defined to characterize the hybrid device (here, the influence of the refractive index change when introducing NCs is ignored and discussed in the Supporting Information), wherein I_{MQW}^{H} represents the integral intensity of MQW emission in the hybrid device. For 546-NCs, it is calculated as high as 94% in the hybrid violet h-LED and 83% in the hybrid blue h-LED. (for other data, see Table S2 in the Supporting Information). It is worth highlighting that owing to the unique device design, the CCE of the hybrid violet h-LEDs is much higher than that previously reported in the literature,[11,29,30] and the effective QY is even higher than that of YAG phosphors.[42]

Figure 3a shows the normalized emission spectra of the bare violet and blue h-LEDs and the absorption and normalized emission spectra of 518-NCs. (for the others, see Figure S2 in the Supporting Information). This indicates that the emission wavelengths of both h-LEDs are in the range of intense NC

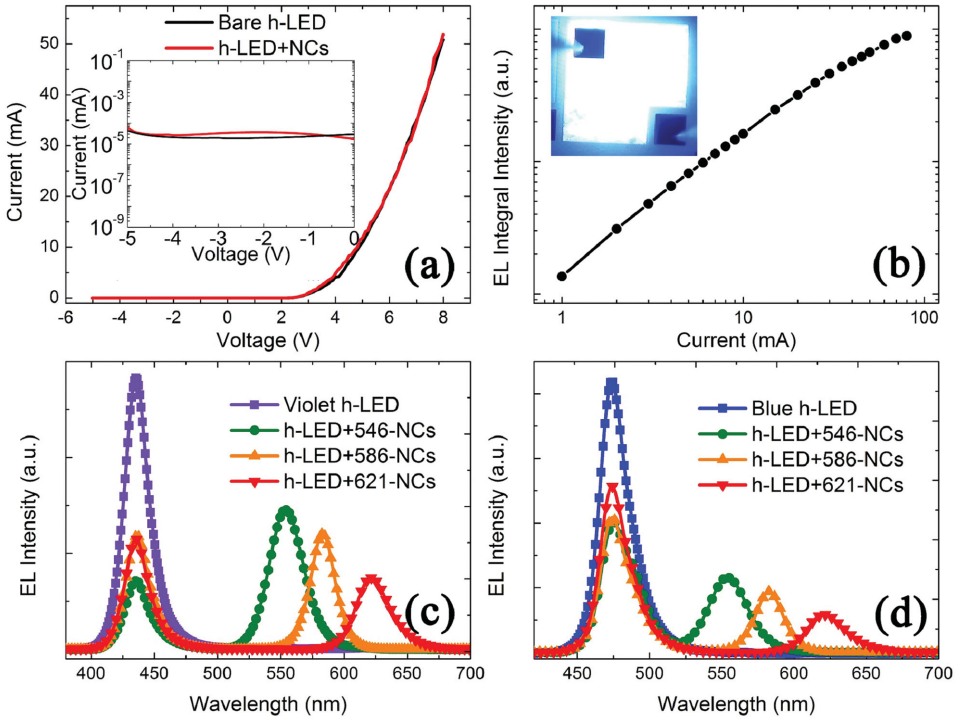

Figure 2. a) *I–V* characteristics of the h-LEDs with and without NCs. The inset is the *I–V* curve at the reverse bias on a logarithmic scale. b) The trend of the EL integral intensity as a function of the injection current. The inset is a CCD image of the bare blue h-LEDs at the injection current of 1 mA. The EL spectra of the hybrid c) violet and d) blue h-LEDs filled with 546-NCs, 586-NCs, and 621-NCs at the injection current of 20 mA, respectively.

absorption, indicating good spectral overlaps of MQWs with the NC absorption and guaranteeing strong coupling between the excitons in MQWs and the absorption dipoles of NCs at the specific wavelength. Figure 3b displays the physical diagram of the NRET process between the InGaN/GaN MQWs and the NCs along with the relaxation process in the hybrid structures. As a result of the geometry, the coupling actually occurs between the excitons in MQWs (dot) and a 2D-like assembly of NCs (plane), which in fact act as a 1D confined structure.[1,22] As shown, by optical pumping or current injection, carriers are generated, and excitons are distributed in MQWs. These excitons can recombine either radiatively to emit photons or nonradiatively by defects or experience resonant NRET into an assembly of NCs if the excitonic energy of MQWs can match the absorption energy of NCs. After the energy is transferred to NCs, an extremely fast intraband relaxation in NCs will happen at once, removing excitons from resonance with the MQW transition and effectively preventing the back-transfer process.[1] The relaxed excitons in the NCs then primarily recombine radiatively, emitting photons with an energy corresponding to the NC's bandgap. In this geometry, the decay rate of NRET is described as[28,43]

$$k_{ET} = k_{MQW}\frac{\beta\pi\sigma_{NC}R_0^6}{2d^4} = k_{MQW}\left(\frac{R_0'}{d}\right)^4 \quad (1)$$

where k_{MQW} is the de-excitation rate of the MQW excited state in the absence of NCs, σ_{NC} is the NC's surface density, R_0 and R_0' are the point-to-point and modified Förster radii, respectively, here radius is defined as the separation distance between donors and acceptors when the NRET efficiency becomes equal to 50%; d is the separation between the excitons in the MQWs and NCs; and β is the modified factor. A detailed derivation of Equation (1) is included in the Supporting Information.

To explore the carrier dynamics and reveal the NRET process, the RT temporal evolution of PL in hybrid violet/blue h-MQWs, as well as isolated h-MQWs and NCs, is monitored, as shown in Figure 3c,e. (see Figure S3 in the Supporting Information.) All recorded PL signals correspond to the peak emission wavelength of h-MQWs or NCs. It can be seen that the excitons in both hybrid h-MQWs decay significantly faster (approximately four times faster, according to the fits discussed later) compared with their isolated counterparts, accounting for an existing NRET process that introduces an additional decay channel for the excitons in the hybrid h-MQWs, as explained in Figure 3b. It is worth mentioning that similar time-resolved photoluminescence (TRPL) measurements are performed on blue h-MQWs coated with an organic material (polymethyl methacrylate, PMMA), which has no absorption at the InGaN/GaN MQW emission wavelength. (see Figure S5 in the Supporting Information). It is found that there is no change in the decay lifetime of blue h-MQWs coated with PMMA compared with bare h-MQWs, further confirming that the decay change of hybrid h-MQWs is due to the NRET process instead of the change in the refractive index of nanoholes.

For isolated h-MQWs, the decay curves can be simply fitted with a double exponential decay as follows[2,31,34]

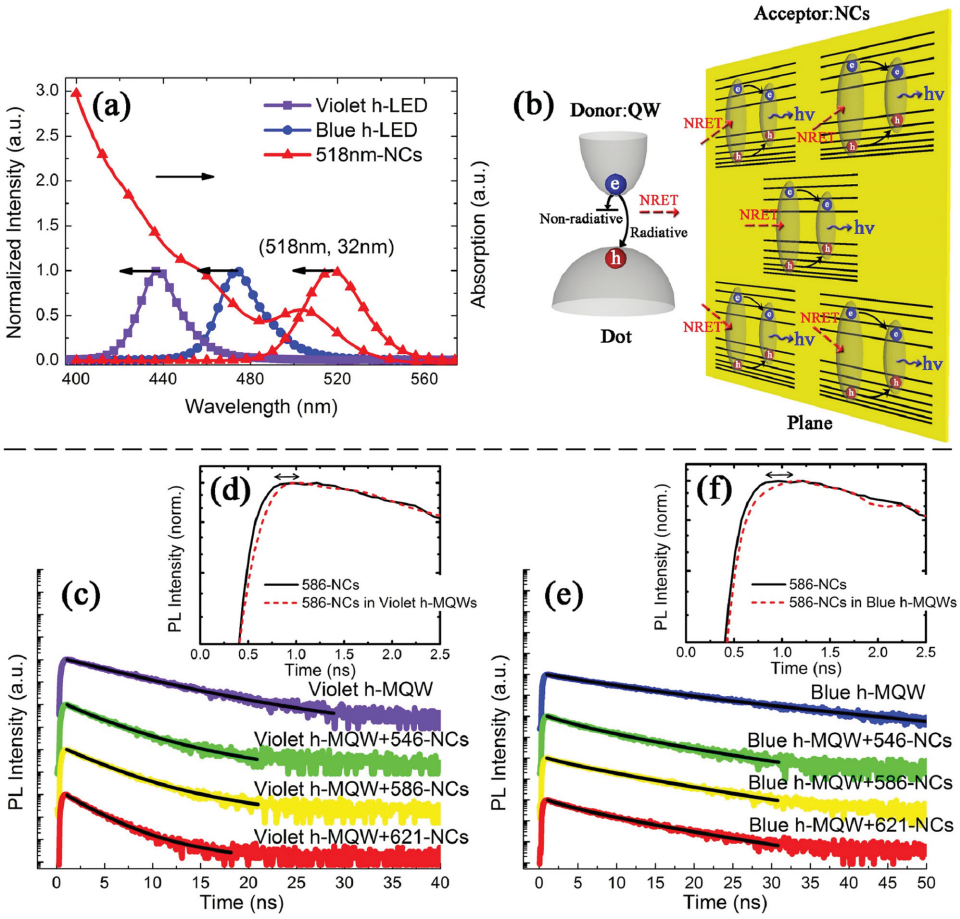

Figure 3. a) The normalized emission spectra of bare violet and blue h-LED and the absorption and normalized emission spectra of 518-NCs. b) The physical schematic diagram of a NRET process. c,e) The decay curves of violet and blue h-MQWs filled with 546-NCs, 586-NCs, and 621-NCs, respectively. d,f) The decay curves of 586-NCs on the glass substrate and in violet/blue h-MQWs, respectively.

$$I_{MQW} = A_1 \exp\left(-k_{MQW1} \cdot t\right) + A_2 \exp\left(-k_{MQW2} \cdot t\right) \quad (2)$$

where A_1 and A_2 are constants and k_{MQW1} and k_{MQW2} are the fast and slow components of the decay rate of excitons in isolated MQWs, respectively.

For hybrid h-MQWs filled with NCs, the carrier dynamics are more complicated. Those excitons in h-MQWs arriving at sidewalls of nanoholes (within the Förster radius) can undergo NRET at a faster decay rate, but those excitons further away cannot (normally more than twice the Förster radius). They still behave at their original decay rate as in the case of h-MQWs alone. As a result, the transient decay of hybrid h-MQWs can be fitted with the following equation[30,31,44]

$$I_{MQW}^{H} = \sum_{i=1,2} A_i \exp\left(-\left(k_{ETi} + k_{MQWi}\right) \cdot t\right) + \sum_{i=1,2} B_i \exp\left(-k_{MQWi} \cdot t\right) \quad (3)$$

where the first two terms describe the decay dynamics of the excitons in h-MQWs that undergo the NRET process, and the last two terms describe the decay dynamics of the excitons that do not undergo the NRET process. Because the ratio of the NRET rates corresponding to the components of the high and low oscillator strength scales approximately with the ratio of the fluorescence decay rates of the fast and slow components, respectively, it can be obtained that[44]

$$\frac{k_{ET1}}{k_{ET2}} = \frac{k_{MQW1}}{k_{MQW2}} \quad (4)$$

which should also be considered when fitting the decay dynamics of h-MQWs. Moreover, the NRET efficiency is determined by

$$\eta_{ET} = \frac{k_{ET1}}{k_{ET1} + k_{MQW1}} = \frac{k_{ET2}}{k_{ET2} + k_{MQW2}} \quad (5)$$

which means that because the decay rate of NRET is much larger than that of exciton recombination in h-MQWs, carriers can mostly go through the NRET channel, and high NRET efficiency can be achieved. From the fitting (solid black line in Figure 3c,e), the fastest NRET decay rate k_{ET1} in hybrid h-MQWs (see Table S3 in the Supporting Information) reaches 1.01 ns^{-1}, which is four times faster than the corresponding fast decay rate of isolated h-MQWs, 0.25 ns^{-1}, competing with exciton recombination in h-MQWs. In addition, owing to the minimized distance between h-MQWs and NCs in the hybrid structures, the NRET efficiency is obtained up to 80%, which is as high as other similar hybrid structures reported previously.[2,28,30] Furthermore, it is imperative to investigate the effect of NRET on the emission dynamics of NCs.[10,30,44] The

insets in Figure 3d and f show the rising time of the transient fluorescence decays of 586-NCs on the glass substrate and in violet/blue h-MQWs, respectively, which definitely demonstrate the slowing rising time of NCs in violet/blue h-MQWs compared with that of the isolated ones. Moreover, the fluorescence decays of 586-NCs in violet/blue h-MQWs reveal good agreement with the fitted curves (see Figure S6 in the Supporting Information), unequivocally proving that NRET exists in the hybrid h-LEDs studied here.

It is known that the NRET process mainly depends on the coupling distance d between the MQWs and NCs.[45] By utilizing Equation (1), the average coupling distance d of NRET in the hybrid structures ranges from 5.2 to 7.7 nm, which is smaller than the modified Förster's radius R_0' (see Table S4 in the Supporting Information), implying that the coupling between h-MQWs and NCs is strong enough to achieve a high efficiency of NRET. Moreover, it is noticed that the average coupling distance d is also smaller than a single NC diameter, illustrating that except for the first layer of NCs attached to the sidewalls of h-MQWs, the NCs further away may not undergo NRET. As a result, the nanohole arrays with an emission area 3.5 times larger can have equivalent NRET coupling compared with the nanorod arrays due to the equal area of their sidewalls, which exhibits an advantage of the nanohole-based hybrid structures.

With regard to high-quality hybrid white LEDs, it is important to modify the optical parameters such as the chromaticity coordinates, CCT, and CRI. First, a mathematical model is adopted[46] to simulate violet and blue h-LEDs with different color schemes. The spectral power distributions of hybrid violet/blue h-LEDs are given by (see the Supporting Information)

$$S_{\text{white}}(\lambda) = S_{\text{MQW}}(\lambda) + k_{\text{NC1}} \cdot S_{\text{NC1}}(\lambda) + k_{\text{NC2}} \cdot S_{\text{NC2}}(\lambda) + \cdots \quad (6)$$

where k_{NC1}, k_{NC2}... are the ratios of the peak intensity of NCs to those of LEDs.

Because the CRI of the binary complementary color scheme (h-LEDs + one type of NCs) is low (see Figure S7 in the Supporting Information), hybrid h-LEDs with ternary complementary color (h-LEDs + two types of NCs) are considered. **Figure 4**a shows the simulated results plotted in the 1931 CIE chromaticity diagram, the chromaticity coordinates of which approach the blackbody line. Four schemes present good performance among all types of schemes between h-LEDs and NCs, as labeled in Figure 4a. The CRI has arrived at 70–80 and 75–86 for hybrid violet and blue h-LEDs, respectively. Moreover, these points are across CCT areas from 2500 to 10 000 K, revealing that the hybrid h-LEDs can be accessed to change the CCT for various applications. Based on this simulation, two schemes, hybrid violet h-LEDs + 518-NCs + 600-NCs and blue h-LEDs + 546-NCs + 621-NCs, are adopted for experiments and labelled with stars in Figure 4a. Figure 4b exhibits the EL spectra of the two combinations of hybrid devices normalized to the peak intensity of h-LED emission at the injection current of 20 mA. The hybrid violet h-LED has a CRI of

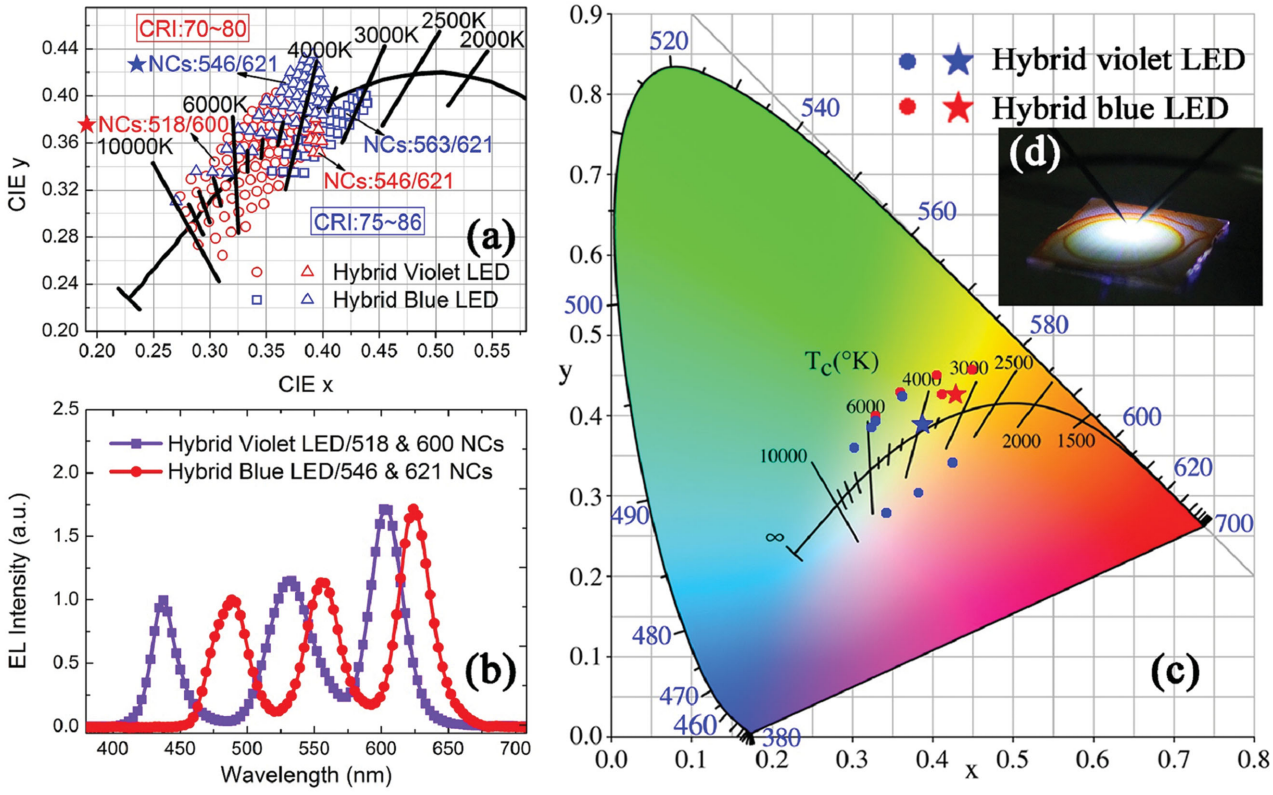

Figure 4. a) Simulated CIE 1931 chromaticity diagram of ternary complementary color hybrid h-LEDs. b) The EL spectra of hybrid violet and blue LEDs with a CRI of 80 and 82, respectively. c) The experiment data locations in the CIE 1931 chromaticity diagram of ternary complementary color hybrid h-LEDs marked with stars in (a). d) The picture of the generated white light of hybrid violet h-LED at the injection current of 20 mA.

80 with T_c = 3888 K, which is located at (0.388, 0.388) in the 1931 CIE chromaticity diagram, whereas the hybrid blue h-LED has a CRI of 82 with T_c = 3318 K, located at (0.429, 0.427) (labeled as blue and red stars in Figure 4c, respectively), both of which are prior to the previous reports.[25,26] The appearance of the generated white light from the hybrid violet h-LED is shown in Figure 4d, exhibiting bright white light and good color rendering of the device. Other experimental data are also plotted as solid dots in Figure 4c, representing hybrid devices with a CRI of more than 70. In addition, these data cover different CCT from 2629 to 6636 K, corresponding to warm white, natural white, and cold white, which agrees with the simulations.

3. Conclusions

In summary, violet/blue h-LEDs have been successfully patterned and fabricated to nanohole arrays by the wafer-level soft UV-curing NIL technique, filled with various wavelength-emitted CdSe/ZnS core/shell NCs to blend white light sources. High CCE (up to 69%) and high effective QY (up to 93%) have been achieved and attributed to an efficient NRET between h-MQWs and NCs, with efficiency as high as 80%. Furthermore, the coupling distance d is smaller than the Förster's radius R_0, which gives convincing evidence for a strong NRET process. Finally, based on theoretical analysis, a series of hybrid h-LEDs with an optimized ternary complementary color scheme has been realized with a high CRI above 70, up to 82, covering different CCT ranging from 2629 to 6636 K corresponding to warm white, natural white, and cold white. This approach is therefore promising to obtain efficient and high-quality white light sources with the advantage of a compatible fabrication process for mass production.

4. Experimental Section

Sample Preparation: Hybrid h-LEDs were fabricated from InGaN/GaN MQW epitaxial wafers grown by metal organic vapor phase epitaxy (MOVPE) on c-plane patterned sapphire substrates. The epitaxy comprised a 2 μm undoped GaN buffer, 3 μm n-type GaN layer, and 15 periods of InGaN/GaN MOWs where well and barrier thicknesses were approximately 3 and 12 nm, respectively, followed by a 50 nm p-type AlGaN layer, and finally a 400 nm thick p-type GaN. The indium compositions were 0.17 (violet) and 0.23 (blue), respectively. The device fabrication process started with depositing a 100-nm-thick ITO film using physical vapor deposition (PVD), a 200-nm-thick silicon dioxide (SiO_2) film using plasma-enhanced chemical vapor deposition and a 30-nm-thick nickel film using PVD again, followed by spin coating one layer of SU8 and another layer of UV resist in turn. A soft UV NIL process was then carried out to produce nanoholes on the UV resist. After the NIL process, the residual UV resist and SU8 layer were etched using a reactive ion etching process with CHF_3 and O_2 gases, followed by an inductively coupled plasma process, and the nanopatterns were consequently transferred to the nickel layer. Then, several steps of photolithography and post-growth etching processes were employed to finish violet/blue h-LEDs. To remove any surface damage generated by the dry-etching process used, all nanohole samples were healed by a careful chemical treatment.[47]

The CdSe/ZnS core/shell NCs (QSP-520, QSP-540, QSP-560, QSP-580, QSP-600, and QSP-620) were purchased from Ocean Nanotech LLC and dispersed in toluene (10 mg mL^{-1}). The hybrid violet and blue h-LEDs were prepared by drop casting the solution of CdSe/ZnS core/shell NCs onto the corresponding h-LEDs, followed by complete evaporation of the solvent under ambient atmosphere.

Characterization and Simulation: The morphology of InGaN/GaN nanoholes and NCs were observed by a JEOL JSM 7000F field emission SEM and a FEI Titan 80–300 TEM. Electrical pumping of the devices was implemented by forward biasing the p–i–n junction of nanoholes with a Keithley 2601 semiconductor parameter analyzer. The hybrid violet and blue h-MQW structures were excited at 405 nm by a picosecond laser (LDH series, Pico Quant) under a very low excitation power density regime (≈1 W cm^{-2}). The time-resolved PL measurements were taken on a time-correlated single-photon counting system with a time resolution of 250 ps. The peak emission from either the MQWs or the NCs was selected using a 0.5-meter monochromator (Princeton Instrument). The systematic optimization for white emission indices was simulated by a self-designed Matlab program.

Supporting Information

Supporting Information is available from the Wiley Online Library or from the author.

Acknowledgments

This work was supported by Special Funds for Major State Basic Research Project (Grant No. 2011CB301900), the National Nature Science Foundation of China (Grant Nos. 61274003, 61422401, 51461135002, and 61334009), the Nature Science Foundation of Jiangsu Province (Grant Nos. BK2011010 and BY2013077), the Solid State Lighting and Energy-saving Electronics Collaborative Innovation Center, the Priority Academic Program Development of Jiangsu Higher Education Institutions, and the Scientific Innovation Research of College Graduate in Jiangsu Province (Grant No. CXZZ12_0052).

Received: July 12, 2015
Revised: October 4, 2015
Published online: December 2, 2015

[1] M. Achermann, M. A. Petruska, S. Kos, D. L. Smith, D. D. Koleske, V. I. Klimov, *Nature* **2004**, *429*, 642.
[2] R. Smith, B. Liu, J. Bai, T. Wang, *Nano Lett.* **2013**, *13*, 3042.
[3] W. R. Liu, C. H. Huang, C. P. Wu, Y. C. Chiu, Y. T. Yeh, T. M. Chen, *J. Mater. Chem.* **2011**, *21*, 6869.
[4] H. P. T. Nguyen, K. Cui, S. Zhang, M. Djavid, A. Korinek, G. A. Botton, Z. Mi, *Nano Lett.* **2012**, *12*, 1317.
[5] E. F. Schubert, *Light-Emitting Diodes*, Cambridge University Press, Cambridge, UK **2006**.
[6] M. Yamada, Y. Narukawa, H. Tamaki, Y. Murazaki, T. Mukai, *IEICE Trans. Electron.* **2005**, *E88-C*, 1860.
[7] Y. J. Hong, C. H. Lee, A. Yoon, M. Kim, H. K. Seong, H. J. Chung, C. Sone, Y. J. Park, G. C. Yi, *Adv. Mater.* **2011**, *23*, 3284.
[8] D. M. Yeh, C. F. Huang, H. S. Chen, T. Y. Tang, C. F. Lu, Y. C. Lu, J. J. Huang, C. C. Yang, I. S. Liu, W. F. Su, *IEEE Photon. Technol. Lett.* **2006**, *18*, 712.
[9] J. J. Rindermann, G. Pozina, B. Monemar, L. Hultman, H. Amano, P. G. Lagoudakis, *Phys. Rev. Lett.* **2011**, *107*, 236805.
[10] S. Chanyawadee, P. G. Lagoudakis, R. T. Harley, D. G. Lidzey, M. Henini, *Phys. Rev. B* **2008**, *77*, 193402.
[11] M. Achermann, M. A. Petruska, D. D. Koleske, M. H. Crawford, V. I. Klimov, *Nano Lett.* **2006**, *6*, 1396.
[12] S. Nizamoglu, H. V. Demir, *J. Appl. Phys.* **2009**, *105*, 083112.
[13] S. Nizamoglu, E. Mutlugun, T. Özel, H. V. Demir, S. Sapra, N. Gaponik, A. Eychmüller, *Appl. Phys. Lett.* **2008**, *92*, 113110.

[14] S. Nizamoglu, G. Zengin, H. V. Demir, *Appl. Phys. Lett.* **2008**, *92*, 031102.
[15] E. Jang, S. Jun, H. Jang, J. Llim, B. Kim, Y. Kim, *Adv. Mater.* **2010**, *22*, 3076.
[16] N. J. Findlay, J. Bruckbauer, A. R. Inigo, B. Breig, S. Arumugam, D. J. Wallis, R. W. Martin, P. J. Skabara, *Adv. Mater.* **2014**, *26*, 7290.
[17] D. V. Talapin, J. Steckel, *MRS Bull.* **2013**, *38*, 685.
[18] W. K. Bae, S. Brovelli, V. I. Klimov, *MRS Bull.* **2013**, *38*, 721.
[19] T. Erdem, H. V. Demir, *Nanophotonics* **2013**, *2*, 57.
[20] Q. Dai, C. E. Duty, M. Z. Hu, *Small* **2010**, *6*, 1577.
[21] H. V. Demir, S. Nizamoglu, T. Erdem, E. Mutlugun, N. Gaponik, A. Eychmueller, *Nano Today* **2011**, *6*, 632.
[22] B. Guzelturk, P. L. H. Martinez, Q. Zhang, Q. Xiong, H. Sun, X. W. Sun, A. O. Govorov, H. V. Demir, *Laser Photonics Rev.* **2014**, *8*, 73.
[23] K. Kim, J. Y. Woo, S. Jeong, C. S. Han, *Adv. Mater.* **2011**, *23*, 911.
[24] S. Bhaviripudi, J. Qi, E. L. Hu, A. M. Belcher, *Nano Lett.* **2007**, *7*, 3512.
[25] S. Nizamoglu, T. Ozel, E. Sari, H. V. Demir, *Nanotechnology* **2007**, *18*, 065709.
[26] C. Dang, J. Lee, Y. Zhang, J. Han, C. Breen, J. S. Steckel, C. S. Seth, A. Nurmikko, *Adv. Mater.* **2012**, *24*, 5915.
[27] H. S. Chen, C. K. Hsu, H. Y. Hong, *IEEE Photon. Technol. Lett.* **2006**, *18*, 193.
[28] B. Guzelturk, S. Nizamoglu, D. W. Jeon, I. H. Lee, H. V. Demir, presented at *Conference on Lasers and Electro-Optics 2012*, New York, May 2012.
[29] F. Zhang, J. Liu, G. You, C. Zhang, S. E. Mohney, M. J. Park, J. S. Kwak, Y. Wang, D. D. Koleske, J. Xu, *Opt. Express* **2012**, *20*, A333.
[30] S. Chanyawadee, P. G. Lagoudakis, R. T. Harley, M. D. B. Charlton, D. V. Talapin, H. W. Huang, C. H. Lin, *Adv. Mater.* **2010**, *22*, 602.
[31] S. Nizamoglu, B. Guzelturk, D. W. Jeon, I. H. Lee, H. V. Demir, *Appl. Phys. Lett.* **2011**, *98*, 163108.
[32] S. Nizamoglu, H. V. Demir, *Appl. Phys. Lett.* **2009**, *95*, 151111.
[33] B. Jiang, C. Zhang, X. Wang, M. J. Park, J. S. Kwak, J. Xu, H. Zhang, J. Zhang, F. Xue, M. Xiao, *Adv. Funct. Mater.* **2012**, *22*, 3146.
[34] B. Liu, R. Smith, J. Bai, Y. Gong, T. Wang, *Appl. Phys. Lett.* **2013**, *103*, 101108.
[35] Q. Wang, J. Bai, Y. P. Gong, T. Wang, *J. Phys. D, Appl. Phys.* **2011**, *44*, 395102.
[36] M. Athanasiou, T. K. Kim, B. Liu, R. Smith, T. Wang, *Appl. Phys. Lett.* **2013**, *102*, 191108.
[37] K. McGroddy, A. David, E. Matioli, M. Iza, S. Nakamura, S. DenBaars, J. S. Speck, C. Weisbuch, E. L. Hu, *Appl. Phys. Lett.* **2008**, *93*, 103502.
[38] X. Guo, J. Hu, Z. Zhuang, M. Deng, F. Wu, X. Li, B. Liu, C. Yuan, H. Ge, F. Li, Y. Chen, *J. Vac. Sci. Technol. B* **2014**, *32*, 06FG06.
[39] Z. Zhuang, X. Guo, G. Zhang, B. Liu, R. Zhang, T. Zhi, T. Tao, H. Ge, F. Ren, Z. Xie, Y. Zheng, *Nanotechnology* **2013**, *24*, 405303.
[40] L. Y. Chen, Y. Y. Huang, C. H. Chang, Y. H. Sun, Y. W. Cheng, M. Y. Ke, C. P. Chen, J. Huang, *Opt. Express* **2010**, *18*, 7664.
[41] R. Xie, U. Kolb, J. Li, T. Basché, A. Mews, *J. Am. Chem. Soc.* **2005**, *127*, 7480.
[42] S. C. Allen, A. J. Steckl, *Appl. Phys. Lett.* **2008**, *92*, 143309.
[43] J. R. Lakowicz, *Principles of Fluorescence Spectroscopy*, Springer, New York **2006**.
[44] S. Chanyawadee, R. T. Harley, M. Henini, D. V. Talapin, P. G. Lagoudakis, *Phys. Rev. Lett.* **2009**, *102*, 077402.
[45] S. Rohrmoser, J. Baldauf, R. T. Harley, P. G. Lagoudakis, S. Sapra, A. Eychmüller, I. M. Watson, *Appl. Phys. Lett.* **2007**, *91*, 092126.
[46] Y. Ohno, *Opt. Eng.* **2005**, *44*, 111302.
[47] Y. D. Zhuang, C. J. Lewins, S. Lis, P. A. Shields, D. W. E. Allsopp, *IEEE Photon. Technol. Lett.* **2013**, *25*, 1047.